Alkali Subhalides: High Pressure Stability and Interplay between Metallic and Ionic Bonds

Gabriele Saleh[a,*], *Artem R. Oganov*[a,b,c,d]

a Moscow Institute of Physics and Technology, 9 Institutskiy Lane, Dolgoprudny city, Moscow Region, 141700, Russia.

b Skolkovo Institute of Science and Technology, Skolkovo Innovation Center, 3 Nobel St., Moscow 143026, Russia.

c Department of Geosciences and Department of Physics and Astronomy, Stony Brook University, Stony Brook, New York 11794-2100, USA

d School of Materials Science, Northwestern Polytechnical University, Xi'an, 710072, China

ELECTRONIC SUPPLEMENTARY INFORMATION

INDEX

ESI 1. DETAILS ON COMPUTATIONAL METHODS

ESI 1.1 VASP CALCULATIONS

The compounds obtained from USPEX (see section 1.4) were relaxed (geometry optimization) at a number of different pressures in the range 0-350 GPa, along with the structures of pure elements and alkali halides. VASP 5.3.3 version was employed. Note that we neglected the effect of zero point vibrational energy, as it was reported[1] to have a negligible effect on the stability of sodium subchlorides.

For all alkali atoms, all electrons belonging to the valence shell and to the most external core shell were explicitly included in the SCF calculations. Concerning halogens, all valence electrons were treated explicitly. The 'hard' pseudopotential was used for F and Cl. For Br, for which this kind of pseudopotential is not available, the standard VASP PAW pseudopotential was employed.

The following parameters refer to all the VASP calculations. The energy cutoff was set to 1.3 times the highest among the default values assigned by VASP to frozen core configurations of the elements employed in each calculation. The SCF procedure was considered converged when the energy change between two successive SCF cycles was lower than 10^{-4} eV. For geometry optimization, the threshold for convergence was set to 10^{-3} eV. For SCF calculations, the Brillouin zone was sampled with a grid step size of $0.18/2\pi$ Å^{-1}.

In order to avoid the bias introduced by Pulay stress, we reoptimized each structure until cell edges did not vary more than 0.5% during the geometry optimization.

ESI 1.2 CRYSTAL14 CALCULATIONS

Single point calculations, using the optimized geometries obtained from VASP, were performed exploiting CRYSTAL14.[2] For all atoms, we employed a modified version of a triple-zeta plus polarization basis set optimized for solid state calculations[3]. The 'double-polarization' basis were used for all the compounds except high pressure potassium subhalides (R-3m-K_3Br, C2/m-K_3Br and I4/mmm-K_3Cl), for which only by using 'single polarization' basis set was it possible to obtain convergence in the SCF procedure. The exponent of most external functions were increased in order to make the basis set apt for high pressure calculations. In particular, we shrank the most external s, p and d functions for all atoms, whereas for halogens also the second to last d-shell was contracted, in order to avoid linear dependence problems. Contraction coefficients of 1.96 ($=1.4^2$) and 2.25($=1.5^2$) were used for calculations below and above 190 GPa, respectively. For a given pressure, in order to treat all the systems on an equal footing, the same contraction coefficients were used for all the atoms of all the compounds. However, concerning chemical bonding, these contraction coefficients led to unphysical results for those approaches which are heavily basis set dependent, such as Mulliken charges (*e.g.* a Cl→Na charge transfer was observed in most Na_xCl compounds) and projected-DOS (p-DOS). On the contrary, properties depending on charge density and ELF turned out, as expected, to be scarcely affected by the contraction coefficients applied to the diffuse valence functions.

The basis set issue was particularly important for p-DOS analysis. The latter, on the one hand, was used to extract important information about the chemical bonding of the investigated compounds. On the other hand, we observed that the change in contraction coefficients leads to qualitatively different p-DOS. This problem was found to be more important for the decomposition of DOS into atomic contributions, whereas the relative contributions of atomic s-p-d orbitals turned out to be much less affected. For these reasons, we decided, for the evaluation of p-DOS and Mulliken charges, to perform separate (single point) SCF calculations with different contraction coefficients. The latter were chosen according to the following 3 criteria:

1. The new basis must be variationally better than the 'standard' one (*i.e.* the one with fixed 1.96 and 2.25 contraction coefficients described above). In other words, the change of basis set must lead to a better description of the wavefunction.
2. Agreement with valence density. We compared the atomic contributions of p-DOS with visual inspection of the charge density distribution relative to occupied bands having the highest energy (*i.e.*the valence), obtained from VASP. This condition serves to avoid that relatively diffuse functions of one atom (especially anions) increases its contribution to the valence DOS even when the valence density is mostly accumulated far from such atom.
3. Qualitative agreement between Mulliken and Bader charges. Note that we could change the contraction coefficients of the basis sets so as to match the Bader charges exactly. However, this led to a strong mismatch between the p-DOS results and the valence density plots, *i.e.* to a violation of condition 2, especially for the high pressure forms of K_3Cl and K_3Br. We believe that the reason for this is to be sought in the fact that Bader basins are strongly anisotropic, whereas the set of atomic orbitals corresponding to a given angular momentum l is, by definition, spherically symmetric. Therefore, forcing the match between Mulliken and Bader charges might lead to a strong overlap between cations and anions basis functions, which results in the assignation to the anion of charge which is far away from its center (typically the charge relative to the bond among alkali atoms).

In order to satisfy the three criteria above, different contraction coefficients were used for different compounds. However, for all the cases in which a comparison between the p-DOS of two (or more) systems was discussed in the main text, the employed contraction coefficients were the same. In Table 1, we report the contraction coefficients and the corresponding Mulliken charges for the most significant p-DOS plots (similar contraction coefficients were applied for the remaining p-DOS plots). Finally, for compounds displaying Non-Nuclear Maxima (NNM), additional basis functions were placed on the position of NNM. We adopted the basis functions of He atoms taken from ref. 4. The most internal, very contracted s shell was removed. When not otherwise specified, the exponents of the remaining NNM-centered functions were contracted by a factor 1.44.

Table S1. Contraction coefficients applied to the exponent of the most external basis functions for the evaluation of the p-DOS plots

Figure	Coeff. alkali[a]	Coeff. halogen[a]	Mulliken alkali[b]	Mulliken halogen	MullikenNNM[c]
4	1.7	1.2	+0.38, +0.44, +0.44	-0.47	-0.51
5	1.7	1.2	0.33	-0.66	-
8	1.7	1.2	(a) +0.52 (b) +0.46	(a) -0.79 (b) -0.93	(a) -0.76[d] (b) -0.45
S6	1.7	1.2	-0.03, +0.29	-0.55	-
S21	1.3	1.2	(a,b,c) +0.25, +0.17, +0.33 (d,e,f) +0.14, +0.19, +0.27 (g,h) +0.13, +0.15	(a,b,c) -0.75 (d,e,f) -0.60 (g,h) -0.44	-

[a] This is the contraction coefficient put in the input file. It is the square root of the coefficient actually applied by CRYSTAL14

[b] When a crystal structure contains more than one symmetry-independent atom of the same type, the Mulliken charges are given in the same order as in the picture (*e.g.* the first number corresponds to the atom labeled as Na1 in the p-DOS plot). Labels (a), (b) etc. refer to the specific part of the picture.

[c] Mulliken charges relative to the basis functions centered on Non-Nuclear Maxima

[d] No contraction coefficients applied to NNM basis

The basis set reported in ref. 3 does not contain *d*-orbitals for Li. In order to check a possible occupancy of *d*-orbitals, we added a d function whose exponent of the radial function was chosen by imposing its ratio with the most diffuse p function to be the same as for Na.

In general, a very good agreement was observed between the DOS plots obtained from VASP and the ones obtained with CRYSTAL14. Some examples of DOS obtained with VASP are reported in the following picture (to be compared with main text DOS, as mentioned in the caption).

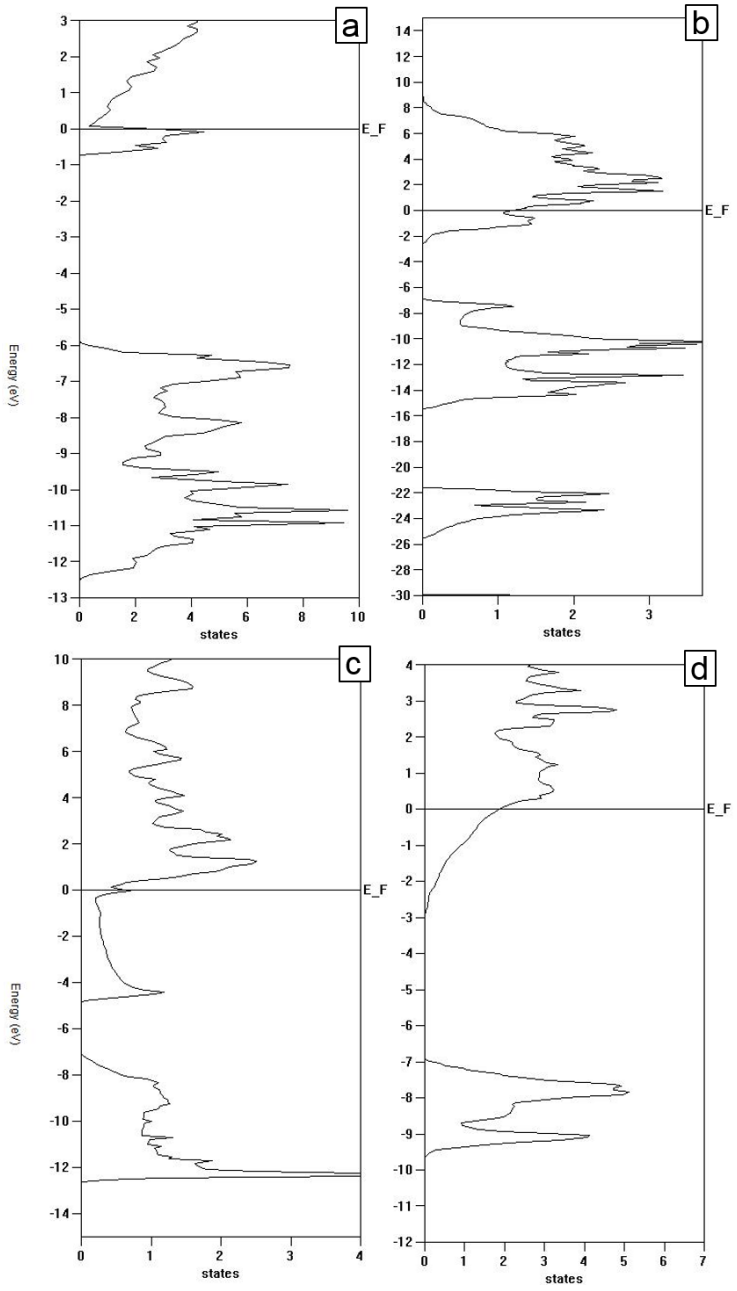

Figure S1. DOS plots obtained from VASP calculations. (a) P4/m-Na_3Cl_2 at 125 GPa (to be compared with Fig. 4) (b) Imma-Na_2Cl at 300 GPa (to be compared with Fig. 5) (c) Pm-3m-Li_3Br at 100 GPa (to be compared with Fig. 8a) (d) Pm-3m-K_3Cl at 100 GPa (to be compared with Fig. 8b)

The reciprocal unit cells were sampled with a 24x24x24 grid for the diagonalization of the Hamiltonian matrices, and with a 48x48x48 grid for the calculation of density matrices and Fermi energies. This was true for all systems but K_3Br, for which the use of such sampling generated a program stop. For this system, 12x12x12 and 24x24x24 grids were used for Hamiltonian matrix diagonalization and density matrix and Fermi energy evaluation, respectively. However, given the fact that both sampling schemes produce very dense grids, we expect our results not to be significantly affected by these changes, especially considering that the CRYSTAL14 calculations were used only for chemical bonding analysis (*i.e.* not for energy

evaluation). For the evaluation of charge density to be used in DFT calculations, we employed the following input, corresponding to unpruned grids (see ref. 2for a full description of the various parameters)

RADIAL

1

x

99

ANGULAR

1

9999.0

13

where x was 3.5 for calculations up to 190 GPa and 3.0 for higher pressure. This value defines the radial extension of the atom-centered grids for the density evaluation.

For bielectronic integrals (TOLINTEG option), we used the keyword TOLINTEG=12,12,12,12,22 for all the systems. In a nutshell, the first two numbers define the truncation threshold for the evaluation of Coulomb series, while the last three numbers refer to the exchange series. The first three numbers refer to the overlap between basis functions (1st and 3rd) or change density distributions (2nd) assigned to a given atom: the summation is truncated when such values becomes lower than $10^{-TOLINTEG}$. The last two numbers, instead, define how many cells are involved in the evaluation of exchange integrals. See ref 2, pag. 276-279 and references therein for a full description of the TOLINTEG parameters. Note that the adopted numbers are roughly doubled with respect to the default values adopted by CRYSTAL14.

ESI 1.3 DETERMINATION OF ZERO-FLUX SURFACES OF ELF AND CHARGE DENSITY

The determination of zero-flux surfaces of charge density (*i.e.* the boundaries of the so-called 'Bader's basins') and the integration of properties within them was carried out by means of the program TOPOND[5], now implemented as a routine in CRYSTAL14. The algorithm developed by T. A. Keith was used: outside the so-called 'β-sphere', 64, 48 and 120 points were used for φ, θ and radial directions, respectively (the meaning of these parameters is described in ref. 5 and references therein). The ray of the β-sphere was taken as 80% of the distance between the nucleus and the closest bond critical point. The integration inside such spheres was performed by doubling the number of points set as default in TOPOND. The integration of quantities within ELF zero-flux surfaces was performed by means of the code critic2[6], exploiting the grid-based Yu-Trinkle algorithm[7]. We used TOPOND to produce very fine grids of charge density and ELF, and converted them into 'cube' format by exploiting the code 'NCImilano'[8]. The grids, spanning the whole unit cell, had a step-size comprised between 0.005 Å and 0.02 Å. The negligibility of errors associated to the numerical integration was checked by comparing the sum of charges and volumes of the basins with the

number of electrons and volume of the unit cell. None of the systems investigated showed a deviation greater than 0.5%.

ESI 1.4 USPEX CALCULATIONS

The crystal structure predictions were carried out within the evolutionary approach implemented in the code USPEX[9]. The philosophy behind the USPEX approach is to find the lowest enthalpy structure on the potential energy surface of a given system by mimicking Darwinian evolution. A number of crystal structures (individuals) form the population of a given generation. Initial structures, *i.e.* the ones forming the first generation, are generally produced randomly (when 'seeds' technique is not used, see *infra*), whereas successive generations are produced by both creating new random structures and by exploiting the most promising structures (*i.e.* the ones having the lowest enthalpy) of the previous generations in order to produce new individuals. The latter process is carried out by applying heredity, softmutation, permutation and transmutation operators (see ref. 9 for the definition of these terms). Moreover, the best individuals (*i.e.* the lowest-enthalpy structures) are automatically passed to the next generation. In our calculations, each generation included 80 individuals in the first generation and 40 in the successive ones. The lowest enthalpy structure was usually found within the first 30 generations (15 when the 'seeds' technique was exploited). For each A_3Y compound, we performed USPEX calculations at 100, 200 and 350 GPa. When starting a new calculation, the most stable structures of the calculation on the same compound at a different pressure were given as input ('seed' technique, see ref. 9). 40 and 25 generations were done for unseeded and seeded calculations, respectively. In addition to the UPSEX runs above mentioned, we also carried out the following additional calculations:

- Variable composition calculations on Na_xCl system at 250 and 125 GPa (140 and 90 individuals for first and successive generations, respectively. 70 generations).
- K_3Br at 50 GPa
- K_3Cl at 40 and 10 GPa
- KBr, KF and NaBr at 200 GPa
- Li_3Br at 60 GPa
- Na_3Br at 50 GPa
- Na_4Cl_3 at 150 GPa

ESI 2. STRUCTURES AND PHONON DISPERSION CURVES FOR THE NEWLY DISCOVERED Na_xCl COMPOUNDS.

In the following, we report the crystal structures (Unit cells in 'POSCAR' format used by VASP) of the 3 newly discovered Na_xCl compounds.

Na_3Cl, $P2_1/c$ space group, 200 GPa

```
Na Cl
   1.0
     5.5287208872914730    0.0000000000000000    0.0000000000000000
     0.0000000000000000    5.1629137717763971    0.0000000000000000
    -2.3912009157014751    0.0000000000000000    4.5918129596164761
  Na  Cl
  12   4
Direct
  0.8328345317875643  0.8680810501075643  0.0317115208758296
  0.1671654682124357  0.1319189498924357  0.9682884791241704
  0.1670645872902052  0.6311990941736390  0.2026668999577286
  0.7365822055624160  0.5001225317048064  0.1165630003120666
  0.8328345317875643  0.6319189498924357  0.5317115208758296
  0.1671654682124357  0.3680810501075644  0.4682884791241704
  0.8329354127097948  0.1311990941736390  0.2973331000422714
  0.8329354127097948  0.3688009058263610  0.7973331000422714
  0.1670645872902052  0.8688009058263610  0.7026668999577286
  0.2634177944375840  0.0001225317048064  0.3834369996879334
  0.2634177944375840  0.4998774682951936  0.8834369996879334
  0.7365822055624160  0.9998774682951936  0.6165630003120666
  0.4996448618016432  0.8303212334701802  0.1719565236282015
  0.5003551381983568  0.3303212334701802  0.3280434763717985
  0.5003551381983568  0.1696787665298198  0.8280434763717985
  0.4996448618016432  0.6696787665298198  0.6719565236282015
```

Na_3Cl, R-3m space group, 300 GPa

```
Na Cl
   1.0
     4.2899665348734484    0.0000000000000000    0.0000000000000000
    -2.1449832674367242    3.7152200005855072    0.0000000000000000
     0.0000000000000000    0.0000000000000000   21.1555556985518116
  Na  Cl
  36  12
Direct
  0.4899038345267129  0.5100961654732871  0.8718208485784381
  0.5092360326770576  0.4907639673229424  0.7079979252826948
  0.8434294988066204  0.1565705011933796  0.7948458180882285
  0.8240973006562757  0.1759026993437243  0.9586687413839718
  0.4899038345267129  0.9798076690534259  0.8718208485784381
  0.8240973006562757  0.6481946013125514  0.9586687413839718
  0.5092360326770576  0.0184720653541153  0.7079979252826948
  0.8434294988066204  0.6868589976132408  0.7948458180882285
  0.3518053986874486  0.1759026993437243  0.9586687413839718
  0.3131410023867592  0.1565705011933796  0.7948458180882285
  0.0201923309465741  0.5100961654732871  0.8718208485784381
  0.9815279346458847  0.4907639673229424  0.7079979252826948
  0.1565705011933796  0.8434294988066204  0.2051541819117715
  0.1759026993437243  0.8240973006562757  0.0413312586160282
  0.5100961654732870  0.4899038345267129  0.1281791514215618
  0.4907639673229425  0.5092360326770575  0.2920020747173051
  0.1565705011933796  0.3131410023867591  0.2051541819117715
  0.4907639673229425  0.9815279346458847  0.2920020747173051
  0.1759026993437243  0.3518053986874486  0.0413312586160282
```

0.5100961654732870 0.0201923309465741 0.1281791514215618
0.0184720653541153 0.5092360326770575 0.2920020747173051
0.9798076690534259 0.4899038345267129 0.1281791514215618
0.6868589976132408 0.8434294988066204 0.2051541819117715
0.6481946013125515 0.8240973006562757 0.0413312586160282
0.8232371678600463 0.1767628321399537 0.5384875152451047
0.8425693660103910 0.1574306339896090 0.3746645919493614
0.1767628321399537 0.8232371678600462 0.4615124847548953
0.1574306339896090 0.8425693660103909 0.6253354080506384
0.8232371678600463 0.6464743357200926 0.5384875152451047
0.1574306339896090 0.3148612679792180 0.6253354080506384
0.8425693660103910 0.6851387320207819 0.3746645919493614
0.1767628321399537 0.3535256642799074 0.4615124847548953
0.6851387320207819 0.8425693660103909 0.6253354080506384
0.6464743357200925 0.8232371678600462 0.4615124847548953
0.3535256642799074 0.1767628321399537 0.5384875152451047
0.3148612679792180 0.1574306339896090 0.3746645919493614
0.6666666666666666 0.3333333333333333 0.2132234200284988
0.6666666666666666 0.3333333333333333 0.0438301503671658
0.6666666666666667 0.3333333333333333 0.6228365162995009
0.6666666666666667 0.3333333333333333 0.4534432466381678
0.3333333333333333 0.6666666666666666 0.5465567533618321
0.3333333333333333 0.6666666666666666 0.3771634837004991
0.3333333333333335 0.6666666666666666 0.9561698496328341
0.3333333333333335 0.6666666666666666 0.7867765799715012
0.0000000000000000 0.0000000000000000 0.8798900866951654
0.0000000000000000 0.0000000000000000 0.7104968170338324
0.0000000000000000 0.0000000000000000 0.2895031829661674
0.0000000000000000 0.0000000000000000 0.1201099133048344

Na_4Cl_3, R-3 space group, 200 GPa

Na Cl
1.0
9.6397808078697160 0.0000000000000000 0.0000000000000000
-4.8198904039348580 8.3482950665288520 0.0000000000000000
0.0000000000000000 0.0000000000000000 4.3132425428647743
Na Cl
24 18
Direct
0.9459485840015417 0.7355266950246946 0.2917749424014582
0.7355266950246946 0.7895781110231529 0.7082250575985418
0.0000000000000000 0.0000000000000000 0.5000000000000000
0.6666666666666666 0.3333333333333333 0.3333333333333333
0.7895781110231529 0.0540514159984583 0.2917749424014582
0.2644733049753054 0.2104218889768471 0.2917749424014582
0.0540514159984583 0.2644733049753054 0.7082250575985418
0.2104218889768471 0.9459485840015417 0.7082250575985418
0.6126152506682083 0.0688600283580278 0.6251082757347916
0.4021933616913613 0.1229114443564863 0.0415583909318751
0.6666666666666666 0.3333333333333333 0.8333333333333333
0.3333333333333333 0.6666666666666665 0.6666666666666666
0.4562447776898195 0.3873847493317916 0.6251082757347916
0.9311399716419720 0.5437552223101805 0.6251082757347916
0.7207180826651249 0.5978066383086387 0.0415583909318751
0.8770885556435137 0.2792819173348751 0.0415583909318751
0.2792819173348751 0.4021933616913613 0.9584416090681249
0.0688600283580278 0.4562447776898195 0.3748917242652086
0.3333333333333333 0.6666666666666666 0.1666666666666665
0.0000000000000000 0.9999999999999999 0.0000000000000000
0.1229114443564863 0.7207180826651249 0.9584416090681249
0.5978066383086387 0.8770885556435137 0.9584416090681249
0.3873847493317916 0.9311399716419720 0.3748917242652086
0.5437552223101805 0.6126152506682083 0.3748917242652086
0.7827197505502016 0.8285423920774072 0.2222042464516648
0.0458226415272056 0.2172802494497984 0.2222042464516648
0.9541773584727944 0.7827197505502016 0.7777957535483352

0.2172802494497984 0.1714576079225928 0.7777957535483352
0.1714576079225928 0.9541773584727944 0.2222042464516648
0.8285423920774072 0.0458226415272056 0.7777957535483352
0.4493864172168682 0.1618757254107406 0.5555375797849981
0.7124893081938722 0.5506135827831318 0.5555375797849981
0.6208440251394611 0.1160530838835350 0.1111290868816686
0.8839469161164650 0.5047909412559262 0.1111290868816686
0.8381242745892594 0.2875106918061276 0.5555375797849981
0.4952090587440738 0.3791559748605389 0.1111290868816686
0.1160530838835350 0.4952090587440738 0.8888709131183314
0.3791559748605389 0.8839469161164650 0.8888709131183314
0.2875106918061276 0.4493864172168682 0.4444624202150018
0.5506135827831318 0.8381242745892594 0.4444624202150018
0.5047909412559262 0.6208440251394611 0.8888709131183314
0.1618757254107406 0.7124893081938722 0.4444624202150018

For these three structures, we have performed phonon calculations using the PHONOPY code[10] (interfaced to VASP). The resulting phonon dispersion curves are reported in the following pictures. When not otherwise specified, the same computational settings as described in ESI 1.1 were adopted.

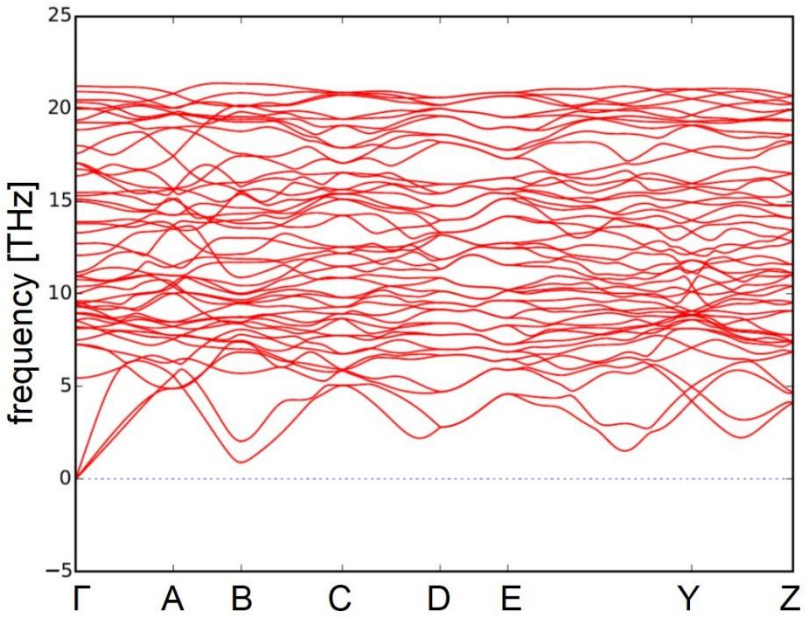

Figure S2. Phonon dispersion curves for $Na_3Cl(P2_1/c$ space group) at 200 GPa. A 2x2x1 supercell (with respect to the cell reported previously in this section) was used.

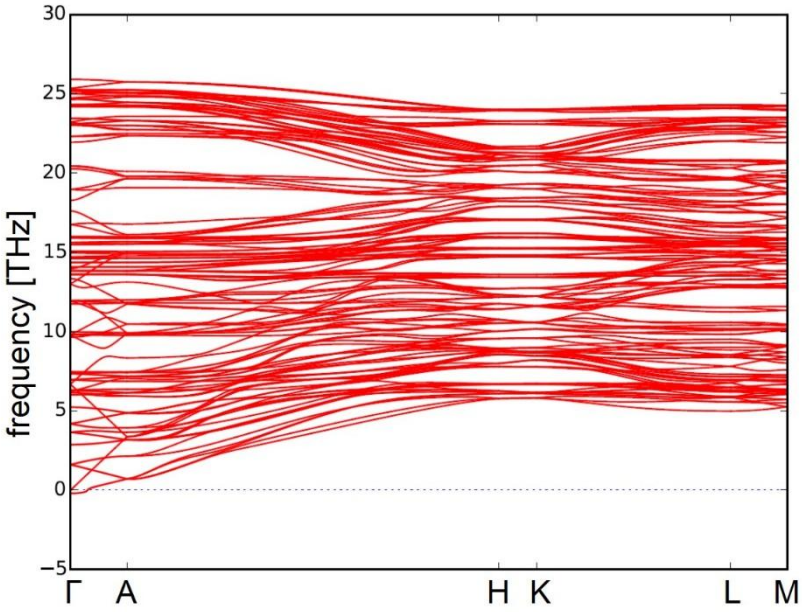

Figure S3. Phonon dispersion curves for Na_3Cl(R-3m space group) at 300 GPa. A 2x2x1 supercell (with respect to the cell reported previously in this section) was used. Note that, since this calculation involved a great number of atoms (192), a coarser sampling of the reciprocal space was used ($0.22/2\pi$ $Å^{-1}$) in order to diminish the computational load.

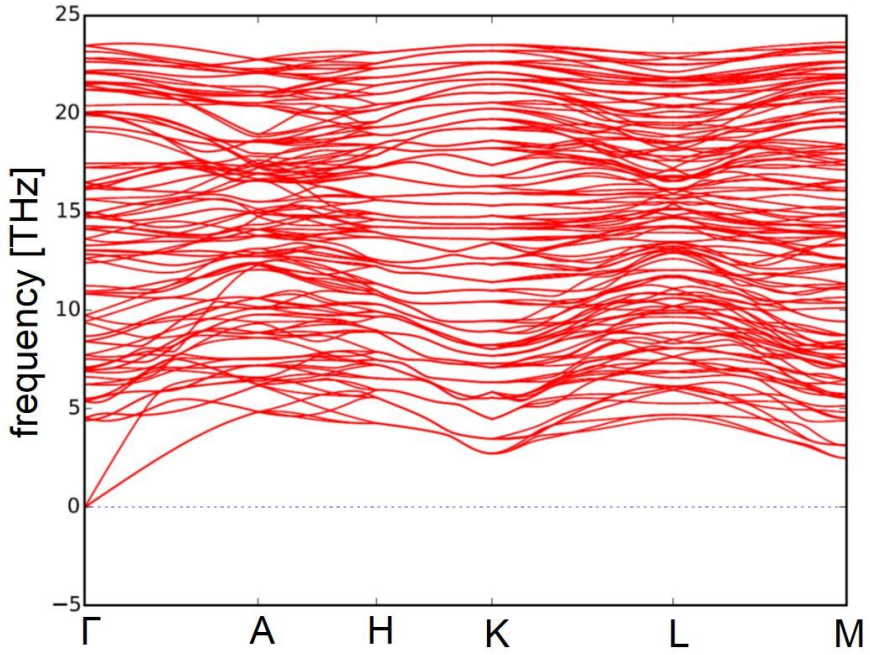

Figure S4. Phonon dispersion curves for Na_4Cl_3(R-3 space group) at 200 GPa. A 1x1x2 supercell (with respect to the cell reported previously in this section) was used.

ESI 3. RESULTS FOR Na_xCl COMPOUNDS NOT SHOWN IN THE MAIN TEXT

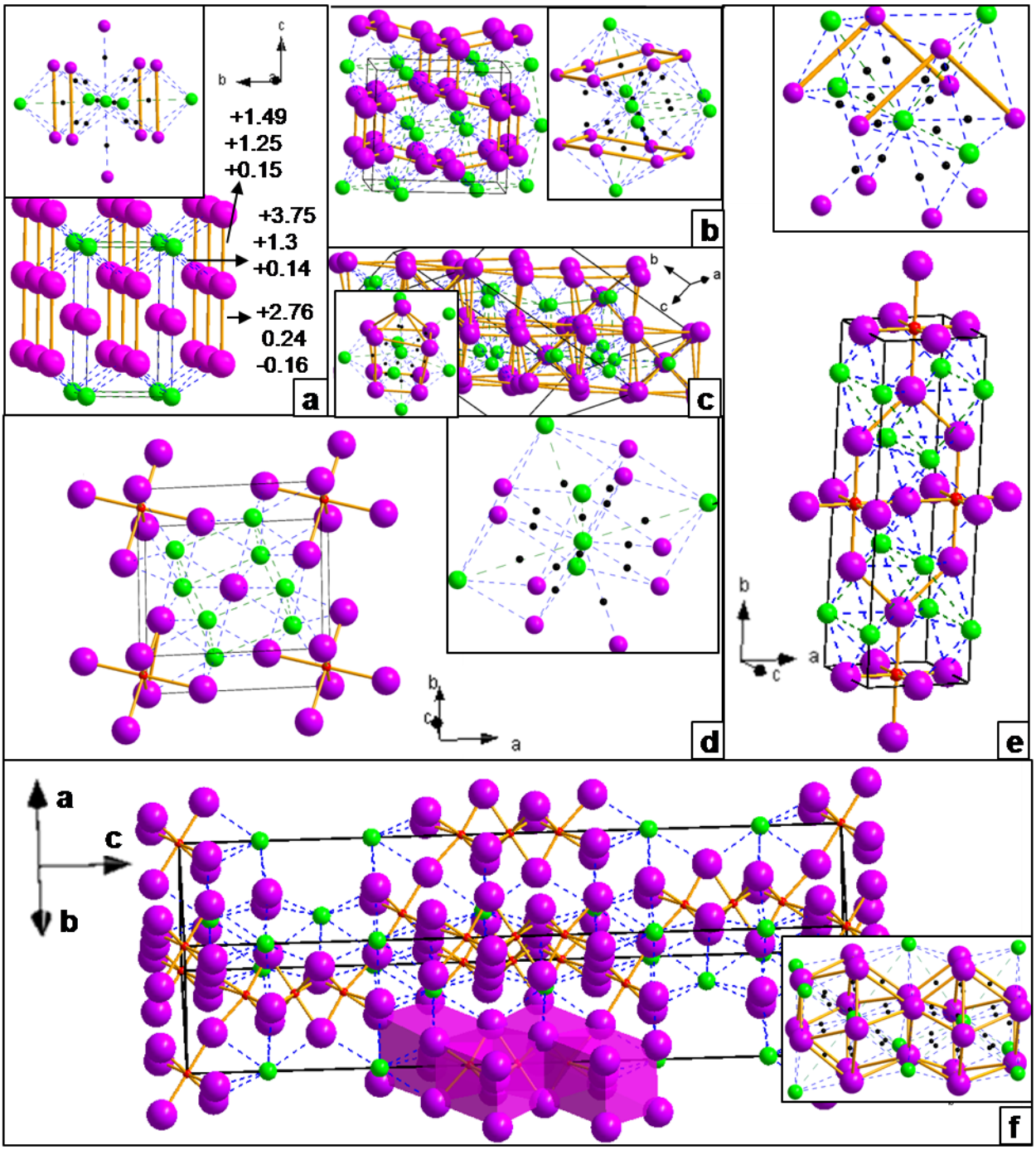

Figure S5. Structures and Bond Critical Points (BCP) for the investigated compounds. (a) P4/mmm-Na_3Cl (b) Imma-Na_2Cl (c) R-3-Na_4Cl_3 (d) P4/m-Na_3Cl_2 (e) Cmmm-Na_2Cl (f) R-3m-Na_3Cl. Bonds, represented as solid sticks (Na-Na) or dashed lines (Na···Cl, Cl···Cl), are drawn only between those atoms connected by a bond paths (except the insets in (c) and the inset of (f), where Na-Na bonds were drawn in order to render the spatial shape of Cl coordination more easily visible). For each picture, the inset shows the coordination sphere of chlorine, and the BCP positions are explicitly indicated by black dots. In this and the following pictures, violet and green spheres represent Na and Cl atoms, respectively. Non-Nuclear Maxima (NNM) of

charge density are represented as small red spheres. NNM can be considered as a manifestation of multicenter bonds and accordingly, atoms involved in the multicenter bond are not directly connected by bond paths but rather a given cluster of atoms form bond paths with the NNM (as it happens in certain metal clusters, *e.g.* Li [11]). In figure (f), we colored some Na-bcc blocks forming the *1D-Na* subalattice showed in Fig. 1e of the main text. Quantities evaluated at the BCPs are reported for bonds of P4/mmm-Na_3Cl at 110 GPa. The three numbers represent, in order, the charge density, the kinetic energy density per electron G(r)/ρ(r) and the total energy density per electron H(r)/ρ(r) (all expressed in a.u.*10^2). Covalent bonds are generally characterized by low G(r)/ρ(r) and negative H(r)/ρ(r) , whereas for closed-shell interactions those values are high and positive[12].

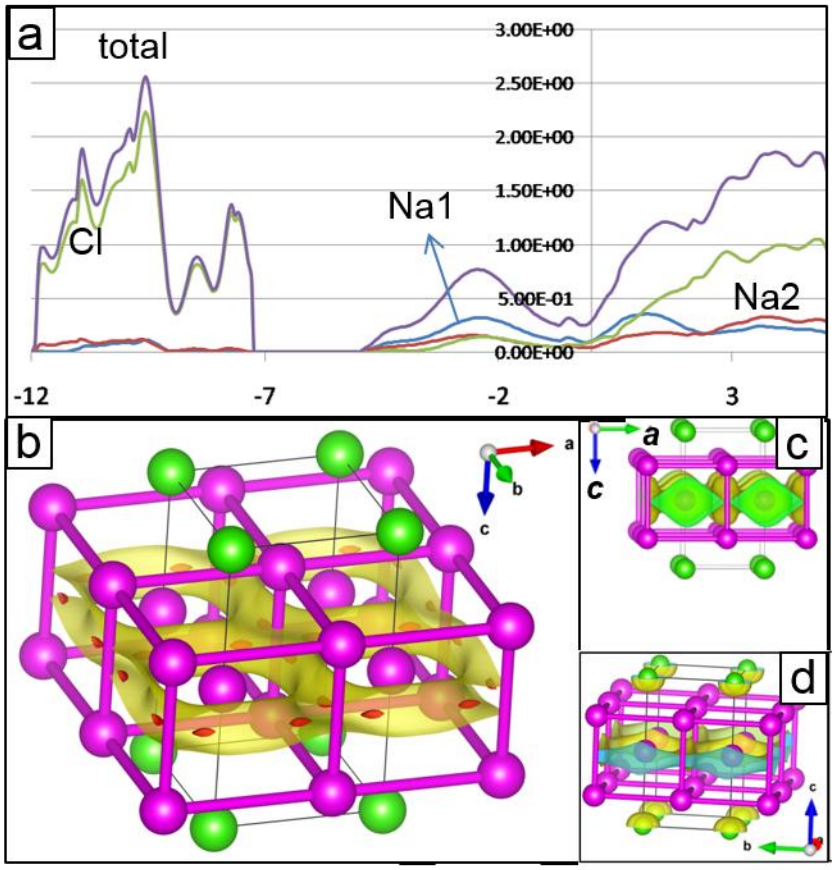

Figure S6. p-DOS (a), partial density plots (b, c), and deformation density (d) for P4/mmm-Na_3Cl at 80 GPa. The unit of measure of the p-DOS plot are eV and eV^{-1} for energy (horizontal axis, values with respect to the Fermi level) and number of states, respectively. In (b) the charge density relative to the valence band (from -5.0 to 0.0 eV) is plotted as two isosurfaces whose isovalues are 0.018 a.u. (yellow) and 0.0215a.u. (red). In (c) the charge density close to the Fermi level (-0.3/0.3 range) is plotted as 0.002 a.u. isosurface. The isosurface represented in (d) was built using an isovalue of +0.0065 a.u.. Note how the deformation density distribution reveals qualitatively the same information obtained from ELF (Fig. 3b of the main text) and

valence density. In particular, an accumulation of charge density in the interstices of the *2D-Na* layers and around Cl atoms is observed.

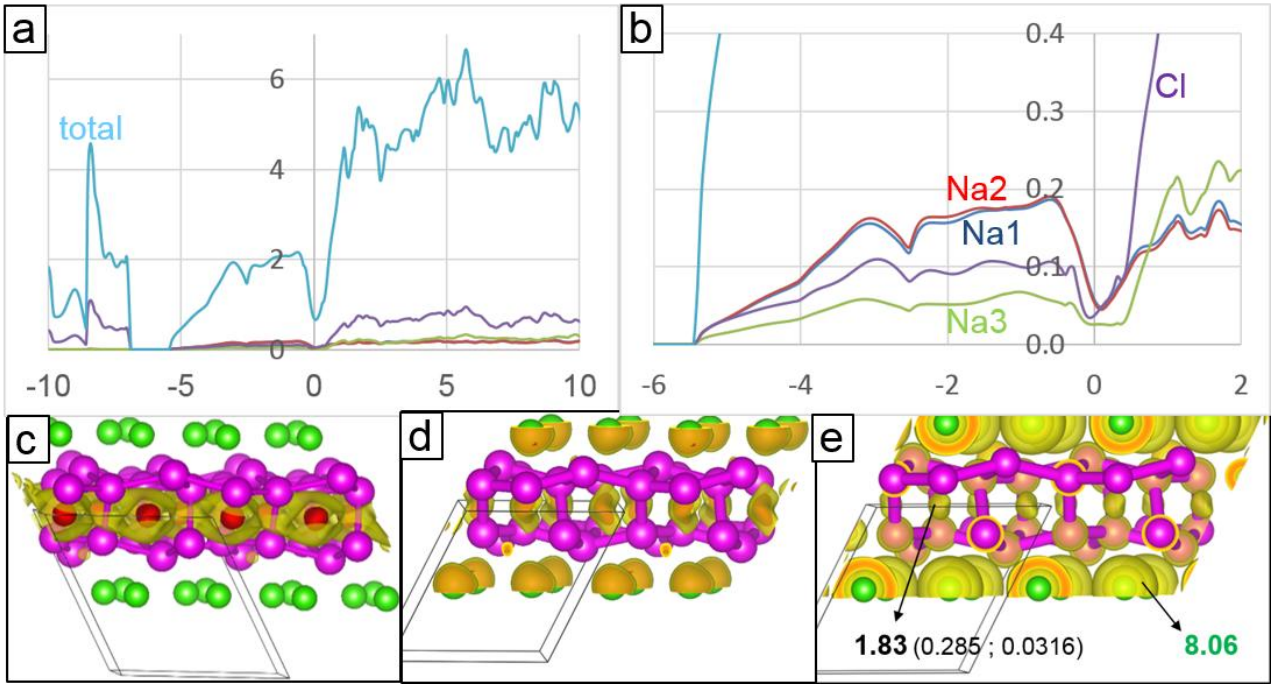

Figure S7. Electronic structure of $P2_1/c$-Na_3Cl at 200 GPa. (a), (b) p-DOS. The unit of measure of the p-DOS plot are eV and eV^{-1} for energy (horizontal axis, values with respect to the Fermi level) and number of states, respectively. (c) valence density (*i.e.* charge density relative to the states in the energy range -5.5/0.0 eV) isosurfaces 0.02 a.u. (yellow) and 0.035 a.u. (red). (d) deformation density; isosurfaces 0.015 a.u. (yellow) and 0.02 a.u. (red). (e) ELF distribution plotted as 0.75 isosurface. Isosurfaces disconnected from atoms are relative to the polysynaptic basins. Their electron population is indicated by black numbers, whereas the two numbers in brackets correspond, in order, to the average ELF and average electron density (in a.u.) inside the basins. Green numbers indicate the valence population of Cl atoms (i.e. the sum of their monosynaptic basins). For comparison, the value of average charge density and average ELF for polysynaptic basins at 200 GPa are 0.285, 0.0322 for P4/m-Na_3Cl_2 and 0.221 0.030 for P4/mmm-Na_3Cl. It is worth pointing out that, despite a thorough search, we did not find any non-nuclear charge density maximum in $P2_1/c$-Na_3Cl 200 GPa. Note how the deformation density distribution reveals qualitatively the same information obtained from ELF and valence density. In particular, an accumulation of charge density in the interstices of the *2D-Na* layers and around Cl atoms is observed.

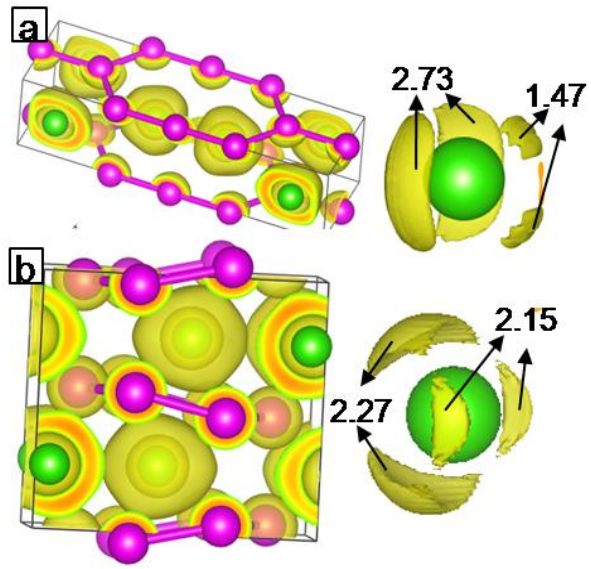

Figure S8. ELF distribution for Cmmm-Na_3Cl_2(a) and Imma-Na_2Cl (b). The enlargement shows the ELF maxima relative to monosynaptic basins of Cl atom and their electron population. The Cl core basins feature a charge of 10.1 electrons (instead of 10 electrons, as found for the Na atoms), perhaps due to numerical integration errors in the determination of basins boundaries. Isosurfaces are drawn using an isovalue of 0.6 for the main picture and 0.84 for the enlargement of Cl atoms.

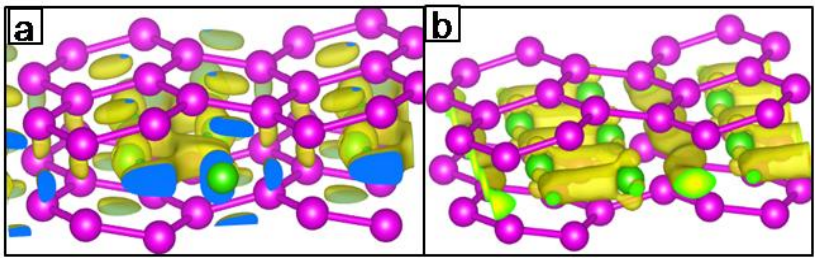

Figure S9. Deformation density (a) and valence charge density (*i.e.* charge density relative to the states in the partially filled band up to the Fermi level) (b) for Imma-Na_2Cl at 300 GPa. Employed isovalues are 0.01 and 0.012 a.u., respectively.

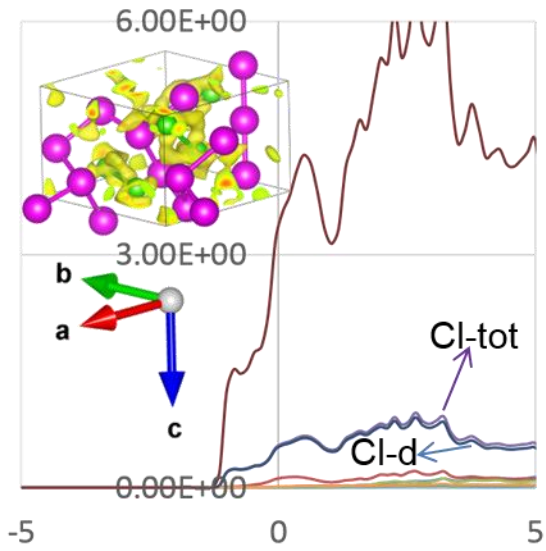

Figure S10. p-DOS near Fermi level for R-3-Na_4Cl_3. Horizontal and vertical axis report Energy (eV, with respect to Fermi level) and number of states (eV^{-1}), respectively. Only significant contributions from the atom- or orbital-projections are labeled (the brown line, instead indicates the total DOS). The inset shows the 0.038 a.u. isosurface of the valence charge density (*i.e.* the charge density corresponding to the energy range -4.0/0.0)

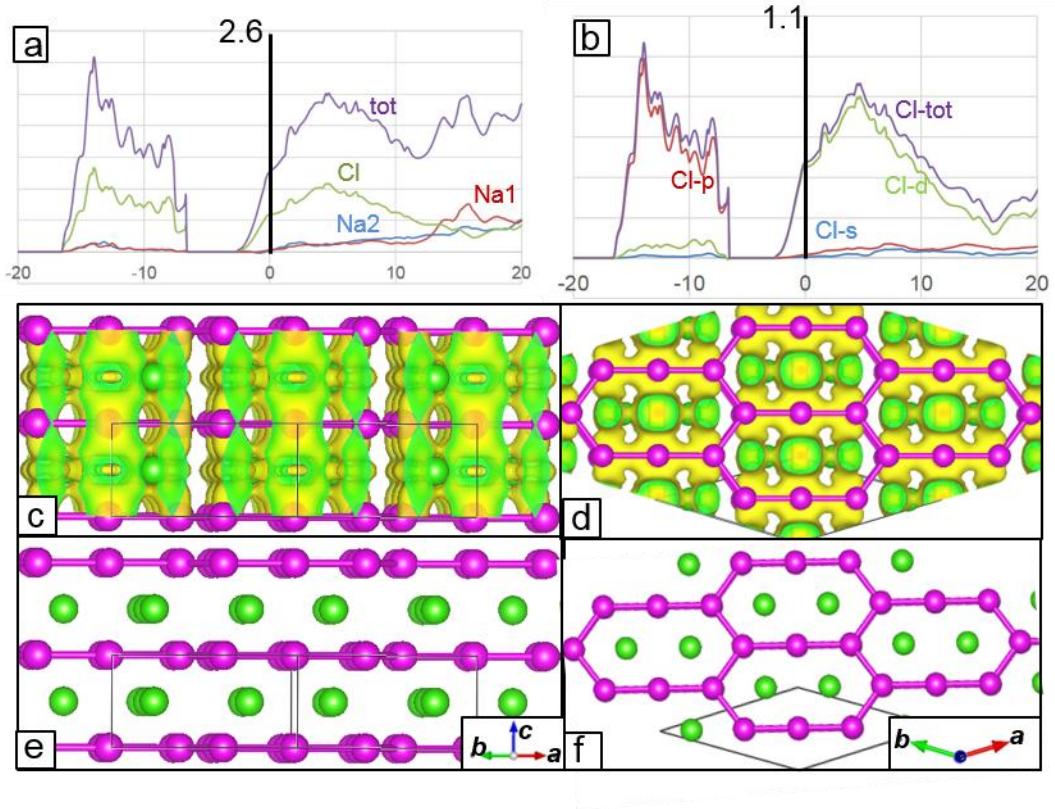

Figure S11. p-DOS (a-b) and charge density near the Fermi level (c-f) for Cmmm-Na_3Cl_2.In (a) and (b), horizontal and vertical axis report Energy (eV, with respect to Fermi level) and number of states (eV^{-1}),

respectively. The picture (c) and (d) represent the 0.003 isosurface of the states near the Fermi level (± 0.3 eV). For sake of clarity, the pictures (c) and (d) are shown without isosurfaces in (e) and (f), respectively.

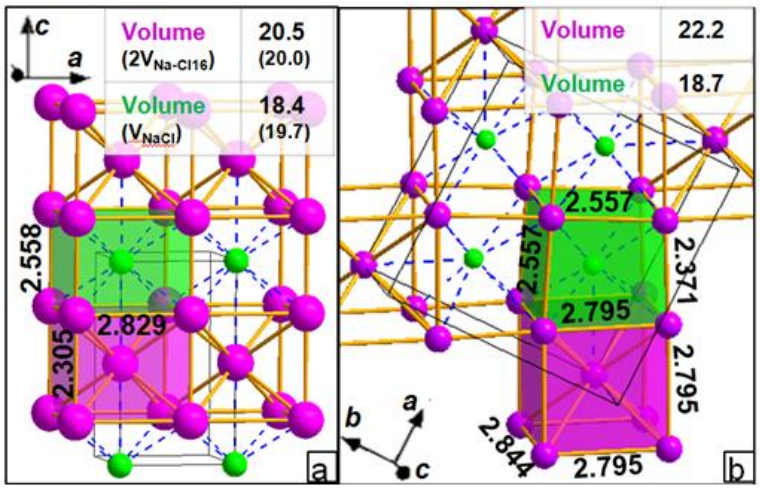

Figure S12. Geometries of P4/mmm-Na_3Cl (a) and P4/m-Na_3Cl_2 (b) at 125 GPa. The partition of the crystal structure into NaCl and Na-bcc blocks is shown, as in Fig. 6 of the main text. The numbers in brackets represent the volume of pure Na and pure NaCl at the same pressure. Distances and volumes are in Å and $Å^3$, respectively.

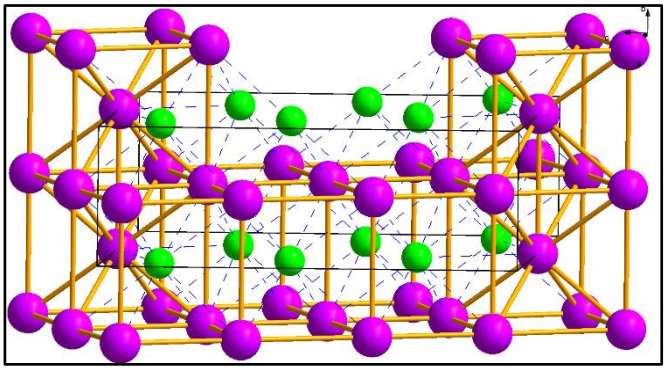

Figure S13. Structure of P2/m-Na_4Cl_3, *i.e.* the lowest enthalpy structure of Na_4Cl_3 (metastable) in the pressure range 125-170 GPa. The *1D-Na* subattice, formed by distorted Na-bcc blocks, is explicitly shown. There are three symmetry-independent Cl atoms, and the number of Na atoms in their coordination sphere is 8,9,9.

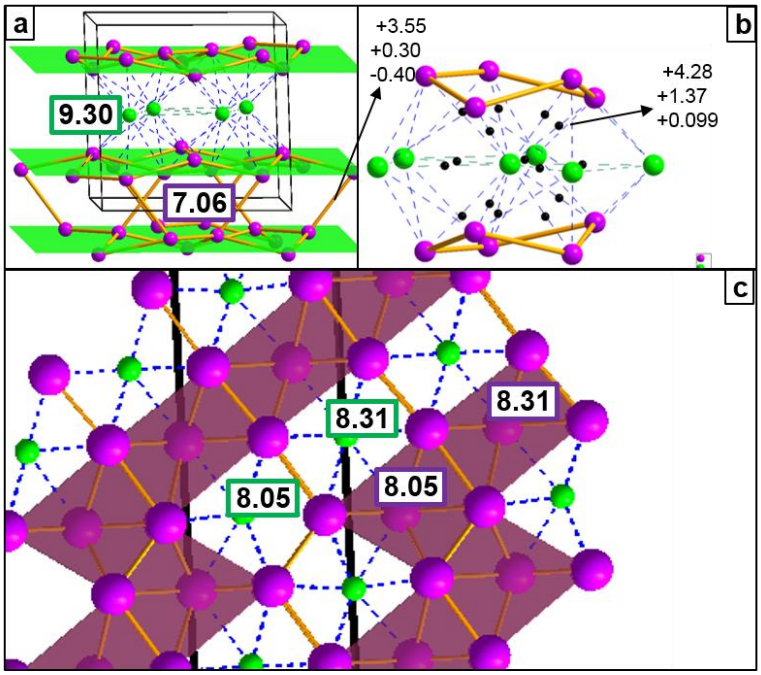

Figure S14. Details of the structures of $P2_1/c$-Na_3Cl (a-b) and R-3m-Na_3Cl (c) at 200 GPa. (a) partitioning of the $P2_1/c$ structure into Na and NaCl layers and relative Volume/atom in $Å^3$. The separating planes have been determined as follows. Of the three symmetry-independent Na, one is almost neutral (see table S2) and was considered as part of the metallic layer, similarly to what happens in the block partitioning of P4/mmm-Na_3Cl. The remaining two symmetry-independent Na atoms, Na2 and Na3 are considered as forming the interphase between Na and NaCl layers. Na2 atoms lie in a plane parallel to the b,c crystallographic plane, and so do Na3 atoms (the two planes are hence parallel to each other). The plane in between the one formed by Na2 atoms and the one formed by Na3 atoms is drawn in the picture and was used as separation between Na and NaCl layers. For comparison, the volume/atom of Na and NaCl blocks of P4/mmm-Na_3Cl at 200 GPaare 8.64 $Å^3$ and 8.02 $Å^3$, respectively. (b) shows the coordination sphere of the Cl atoms of $P2_1/c$-Na_3Cl and the Na-Cl bond critical points are indicated as small black dots. In (a) and (b) we show the values of scalar properties (charge density, the kinetic energy density per electron $G(r)/\rho(r)$ and the total energy density per electron $H(r)/\rho(r)$, all expressed in a.u.*10^2) evaluated at representative bond critical points in the same way as it is done in Fig. S2. In (c), the shape of Na and NaCl blocks does not correspond to any known polyhedron whose volume can be calculated analytically. We evaluated the volume of the two symmetry-independent blocks by approximating them as prisms whose height is perpendicular to the plane of the picture and whose bases are kites (volume 8.05 $Å^3$ in the picture) and squares (volume 8.31 $Å^3$ in the picture). By summing up their volumes, the cell volume is reproduced within 1.27%, hence we concluded that our approximation is reasonable. Note that there are only two symmetry independent polyhedra, therefore Na and NaCl blocks occupy the same volume.

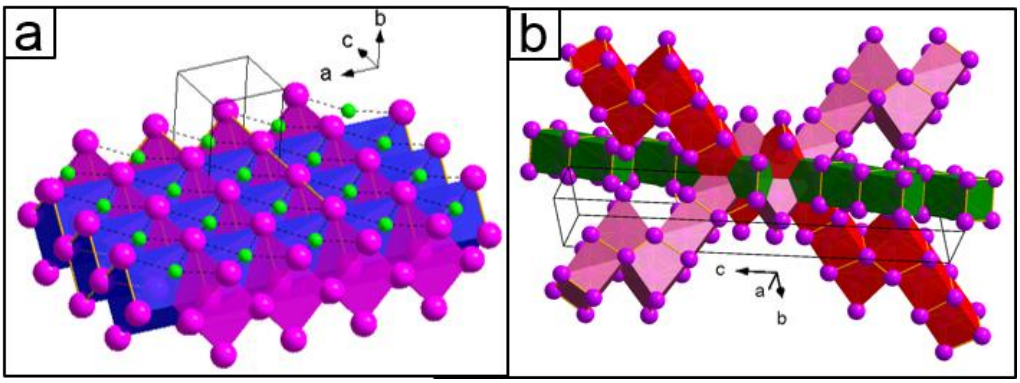

Figure S15. *1D-Na* sublattices in Cmmm-Na_2Cl (a) and R-3m-Na_3Cl (b). In this picture we show how the *1D-Na* strands actually give rise a 2-dimensional (Na_2Cl) and 3-dimensional (Na_3Cl) nets by highlighting them with different colors. Note that, whereas in R-3m-Na_3Cl the three sublattices are symmetry equivalent, in Cmmm-Na_2Cl (a) the Na-bcc blocks forming the blue prisms are more elongated (*e.g.* the height of the two Na-bcc prisms is 2.97 Å and 3.24 Å at 200 GPa).

Table S2. QTAIM atomic properties for sodium subchlorides.

Compound (pressure)	atom	charge	volume [a.u.]
Na_3Cl-P4/mmm (125 GPa)	Na1	0.19	58.3
	Na2	0.36	51.1
	Cl	-0.91	101.8
Na_3Cl-$P2_1/c$ (200 GPa)	Na1	0.16	49.4
	Na2	0.24	46.9
	Na3	0.57	37.4
	Cl	-0.97	87.6
Na_3Cl-R-3m (250 GPa)	Na1	0.57	34.1
	Na2	0.56	34.1
	Cl1	-1.16	86.4
	Cl2	-1.13	86.6
	NNA1	-0.67	15.2
	NNA2	-0.59	14.1
	NNA3	-0.28	6.92
Na_2Cl-P4/mmm (125 GPa, metastable)	Na1	0.24	56.4
	Na2	0.76	37.2
	Na3	0.35	51.1
	Cl	-0.85	99.4
Na_2Cl-Cmmm (200 GPa)	Na1	0.56	36.5
	Na2	0.60	34.6
	Na3	0.66	34.2
	Cl	-0.89	87.5
	NNM	-0.70	18.9
Na_3Cl_2-Cmmm (300 GPa, metastable)	Na1	0.70	30.3
	Na2	0.71	27.8
	Cl	-1.05	77.4
Na_3Cl_2-P4/m (125GPa)	Na1	0.71	37.7
	Na2	0.76	37.6
	Na3	0.48	45.8
	Cl	-0.84	99.0

	NNM	-0.71	25.0
Na_4Cl_3-R-3 (300 GPa)	Na1	0.70	28.7
	Na2	0.69	30.6
	Na3	0.69	28.1
	Cl	-0.93	76.1
Na_2Cl-Imma (300 GPa)	Na	0.66	29.2
	Cl	-1.32	81.6
NaCl-Pm3m (125 GPa)	Na	0.77	36.5
	Cl	-0.77	96.5
NaCl-Pm3m (200 GPa)	Na	+0.77	32.1
	Cl	-0.77	83.73
NaCl-Pm3m (300GPa)	Na	0.75	29.0
	Cl	-0.75	73.2

Table S3. Enthalpy associated to some selected formation energy and phase transitions ofNa_xCl system.

pressure	reactants	product	$\Delta H*10^2$ (eV)	$\Delta pV*10^2$ (eV)	$\Delta U*10^2$ (eV)
80 GPa	2Na(fcc)+NaCl(Pm-3m)	Na_3Cl(P4/mmm)	-5.5	-35.1	29.6
125GPa	1/2Na_3Cl(P4/mmm)+3/2NaCl	Na_3Cl_2(P4/m)	-3.8	-41.8	38.0
150 GPa	Na_2Cl(P4/mmm)[a]	Na_2Cl(Cmmm)	-5.8	-36.7	30.9
150 GPa	1/3Na_3Cl(P4/mmm)+1/3Na_3Cl_2(P4/m)	Na_2Cl(Cmmm)	-3.8	-27.7	23.9
200 GPa	Na_3Cl (P4/mmm)	Na_3Cl($P2_1$/c)	-12.7	-67.5	54.9
250 GPa	Na_2Cl(Cmmm)+2NaCl(Pm-3m)	Na_4Cl_3(R-3)	-54.5	-160.7	106.3
300 GPa	Na_2Cl(Cmmm)	Na_2Cl(Imma)	-2.2	-143	141
300GPa	Na_3Cl_2(P4/m)	Na_3Cl_2(Cmmm)[a]	-21.9	-176	154
300GPa	Na_3Cl($P2_1$/c)	Na_3Cl(R-3m)	-20.9	-56.2	35.3

[a] metastable compound

Table S4. Variation of cell edges of P4/mmm-Na_3Cl with pressure. The a/c cell edges ratio measures the flattening of Na and NaCl blocks described in the main text.

Pressure (GPa)	a/c ratio	a,b (Å)	c (Å)
80	0.577	2.96	5.13
110	0.578	2.86	4.95
135	0.582	2.80	4.82
150	0.584	2.78	4.76
200	0.587	2.69	4.59
250	0.588	2.63	4.47
300	0.590	2.58	4.36

ESI 4. RESULTS FOR ALKALI SUBHALIDES A_3Y (A=Li, Na, K ; Y= F, Cl, Br) NOT SHOWN IN THE MAIN TEXT

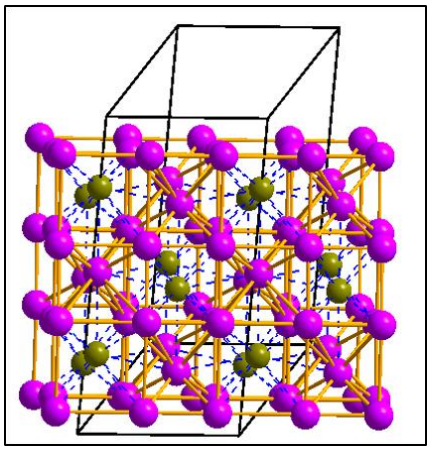

Figure S16. Crystal structure of R-3m-Na_3Br.

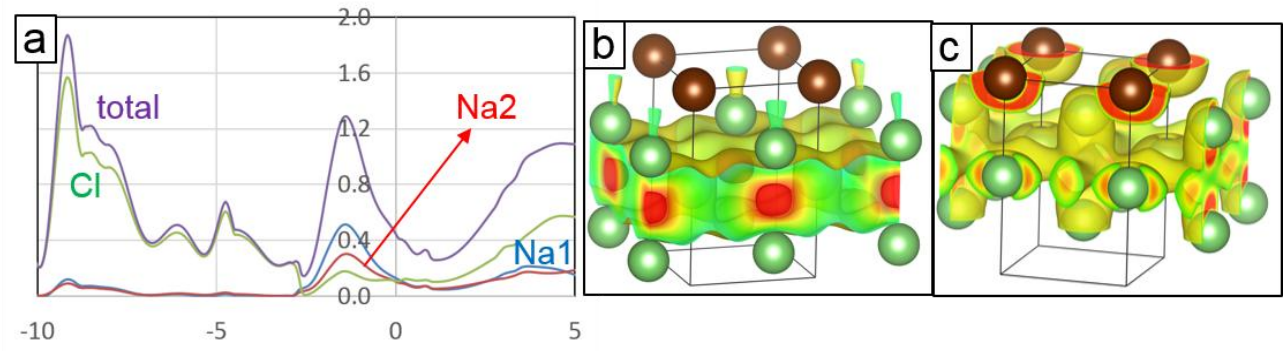

Figure S17. Electronic structure of P4/mmm-Li_3Br at 100 GPa. (a) p-DOS (horizontal axis: energy [eV] with respect to the Fermi level ; vertical axis: states [eV^{-1}]). (b) charge density corresponding to the states in the range -1.86/0.0 eV with respect to the Fermi level (-1.86 eV corresponds to the minimum of Cl contribution and the onset of the increasing contribution of Na1 and Na2). Isosurfaces: 0.01 a.u. (yellow) and 0.03 a.u. (red). (c) deformation density, isosurface 0.005 e/a.u..

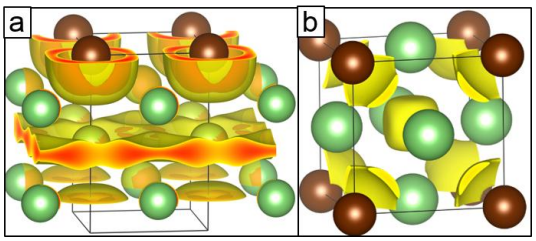

Figure S18. ELF distributions for Li_3Br at 100 GPa. (a) P4/mmm, isovalues 0.6 (yellow) and 0.75 (red) (b) Pm-3m, isovalue 0.75. Note that for P4/mmm we found a non-nuclear charge density maximum within the *2D-Li* sublattice at the crystallographic position 0.5, 0.5, 0.5 (the same being true for P4/mmm-Li_3Cl).

However the formation of such maxima is due to the flatness of the electron density within *2D-Li* layers rather than a particularly strong electron accumulation. Indeed, the greater eigenvalue of the charge density Hessian matrix (the sign of this eigenvalue determines the difference between a maximum and a bond critical point, *i.e.* a first-order saddle) is -0.001 compared to -0.007 for Pm-3m-Li_3Br at the same pressure. As a matter of fact, even at ambient pressure metallic lithium displays the presence of non-nuclear charge density maxima[11].

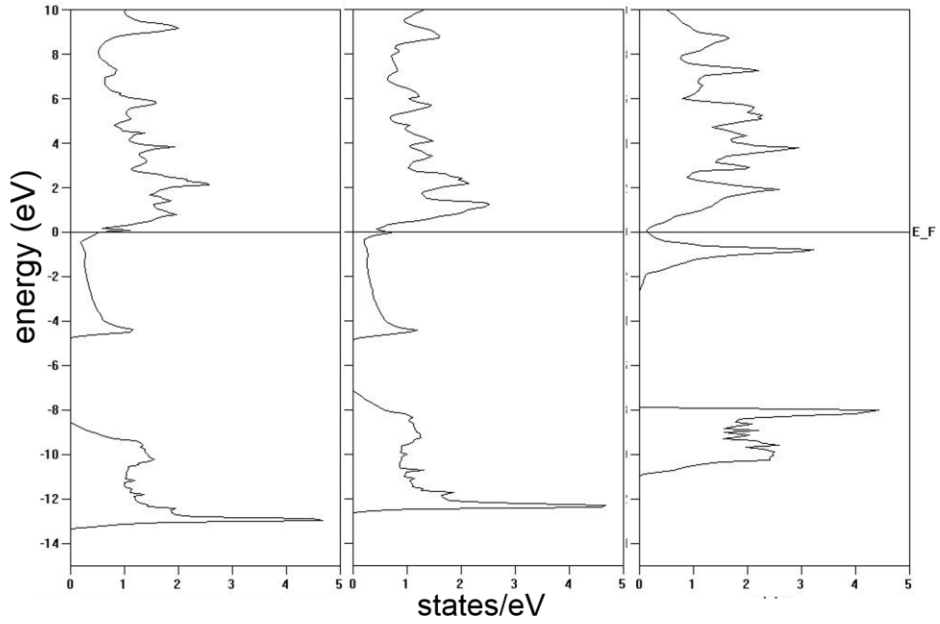

Figure S19. DOS for the Pm-3m structures (obtained from VASP calculations) at 100 GPa. From left to right: Li_3Cl, Li_3Br, Na3Cl.

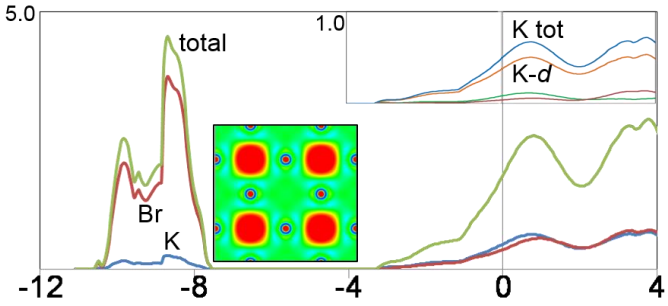

Figure S20. p-DOS for Pm-3m-K_3Br (horizontal axis: energy [eV] with respect to the Fermi level ; vertical axis: states [eV^{-1}]). The inset shows the plot of valence charge density within the 001 plane (2x2 supercell), as done in Fig. 8 of the main text. The color scale is the same as in Fig. 8 of the manuscript, *i.e.* from 0.0 (blue) to 0.01 (red). The upper right inset shows the orbital decomposition of K contribution as obtained from the calculation where no basis were included on the non-nuclear maxima.

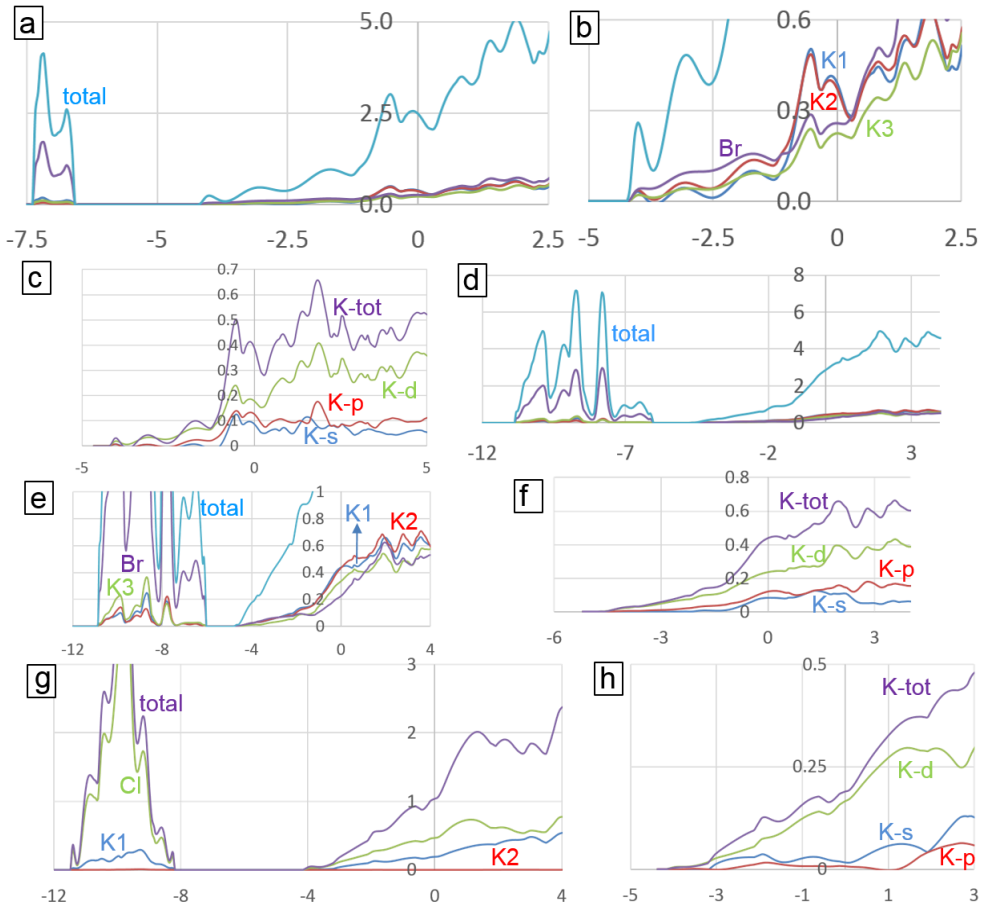

Figure S21. p-DOS for high pressure phases of K_3Cl and K_3Br. Horizontal and vertical axis report Energy (eV, with respect to Fermi level) and density of states (eV^{-1}), respectively. (a) R-3m-K_3Br. Enlargement of the part near the Fermi level shown in (b) whereas the orbital decomposition of K1 contribution to the DOS of K_3Br is shown in (c). (d) C2/m-K_3Br. Enlargement of the part near the Fermi level shown in (e) whereas the orbital decomposition of K1 contribution to the DOS of K_3Br is shown in (f). (g) I4/mmm-K_3Cl. Orbital decomposition of K1 contribution shown in (h).

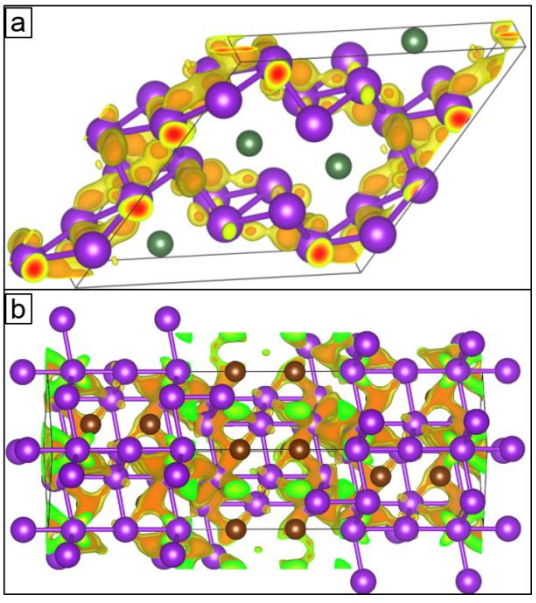

Figure S22.Valence density distribution of C2/m-K_3Br (a) and R-3m-K_3Br (b).Isovalues: 0.011a.u. (yellow) and 0.013a.u. (red). The orientation is similar to Fig. 9b-c of the main text.

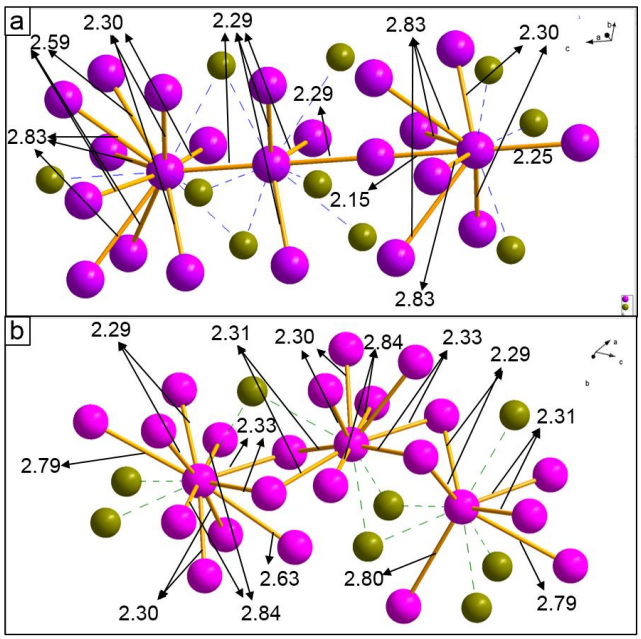

Figure S23. Bond lengths (Å) of all the symmetry-independent K-K bonds K_3Br in R-3m (a) and C2/m (b) phases at 200 GPa. Fo comparison, the 8 shortest K-K bond length in Pm-3m-K_3Br at the same pressure measure 2.447 Å.

Table S5. Energy variation for formation reactions and phase transitions for lithium and sodium subhalides at 100 GPa.

reaction	compound A_3Y	$\Delta H*10^2$ (eV)	$\Delta pV*10^2$ (eV)	$\Delta U*10^2$ (eV)
2A+AY→ A_3Y (P4/mmm)	Li_3Cl	-77.2	-147.9	70.7
	Li_3Br	-22.9	-11.0	-11.9[a]
	Na_3Br	-30.2	-34.3	4.1
A_3Y (P4/mmm)→ A_3Y (Pm-3m)	Li_3Cl	-38.6	-104.2	65.6
	Li_3Br	-87.4	-108.9	21.4
	Na_3Br	-6.5	-45.3	38.8

[a] note that this reaction becomes exothermic well below 100 GPa. At 50 GPa ΔH, ΔpV and ΔU are -0.044 eV, -0.569 eV and +0.526 eV, respectively.

Table S6. Enthalpy variation associated to selected reactions and phase transitions involving K_3Cl and K_3Br compounds

pressure	reactants	product	$\Delta H*10^2$ (eV)	$\Delta pV*10^2$ (eV)	$\Delta U*10^2$(eV)
50 GPa	2K($I4_1$/amd)+KBr (Pm-3m)	K_3Br(Pm-3m)	-1.90	-31.3	29.4
100 GPa	2K(Cmca24)+KCl (Pm-3m)	K_3Cl(Pm-3m)	-13.8	-25.6	11.7
100 GPa	K_3Br(Pm-3m)	K_3Br(C2/m)	-4.4	-9.4	5.0
100 GPa	K_3Cl(Pm-3m)	K_3Cl(I4/mmm)	-0.3	-6.1	5.7

200 GPa	K_3Br(C2/m)	K_3Br(R-3m)	-0.2	-6.8	6.6

Table S7. Volumes [Å^3] of AY and bcc-A blocks for P4/mmm and Pm-3m forms of A_3Y compounds (A=Li,Na and Y= Cl, Br) at 100 GPa. As for sodium subchlorides (Fig. 6 of the main text), the volume reduction associated the formation of the P4/mmm structure is due to the shrinking of AY units (with respect to pure AY). The same effect cannot be observed in the transition from P4/mmm to Pm-3m. This is because in the latter phase, the bcc-A and AY blocks are bound by symmetry to have the same volume. More in details, 4 faces of each block (see Fig. 7 of the main text) are shared between AY andA-bcc blocks (and hence form the A/AY interface). It follows that each edge is shared by 2 AY and 2 bcc-A blocks. Consequently, none of the two blocks types can achieve a volume lower than the other. This geometrical constraint must apply to any A_3Y structure whose A atoms form *1D-A* sublattice (and indeed it holds true for R-3m-Na_3Cl, see Fig. S14). However, from a chemical perspective, the relationship between the increase in the anion-cation coordination and the volume reduction (see Section 3.1 of the main text), can be inferred by observing that the AY blocks are shorter in 2 directions than in the third one (by a factor √2, defined by the space group), and that these two directions exactly correspond to the ones where the 4 additional A···Y contacts (with respect to pure AY alkali halide at the same pressure), are formed.

	P4/mmm		Pm-3m	pure AY	pure A
compound	AY	bcc-A	AY=bcc-A[a]		
Li_3Cl	13.5	14.7	13.3	16.9	12.0
Li_3Br	15.7	15.7	14.9	19.7	12.0
Na_3Br	22.4	22.6	22.2	24.0	21.6

[a] for this structure, the two blocks have the same volume

Table S8. anion/cation core radius ratios for lithium and sodium subhalides (radii taken from ref. 13). For each atom type, the largest value among *s*- and *p*- orbitals was considered.

	F	Cl	Br
Li	0.25	0.52	0.63
Na	0.16	0.33	0.40

Table S9. Atomic properties (QTAIM partitioning) for Pm-3m structures at 100 GPa.

	A atom		B atom		NNM[a]	
A_3Y compound	charge	Volume [bohr^3]	charge	Volume [bohr^3]	charge	Volume [bohr^3]
Li_3Cl	+0.72	16.2	-1.12	102.2	-1.03	28.0
Li_3Br	+0.72	16.6	-1.31	124.5	-0.85	26.0
Na_3Br	+0.58	45.1	-1.02	137.9	-0.70	25.4
K_3Cl	+0.34	81.2	-0.92	101.5	-0.11	3.3
K_3Br	+0.35	77.8	-0.96	112.2	-0.09	2.9

[a]basin associated to the non-nuclear charge density maximum

ESI 5. STRUCTURES AND DENSITY OF STATES FOR Na_6Bi

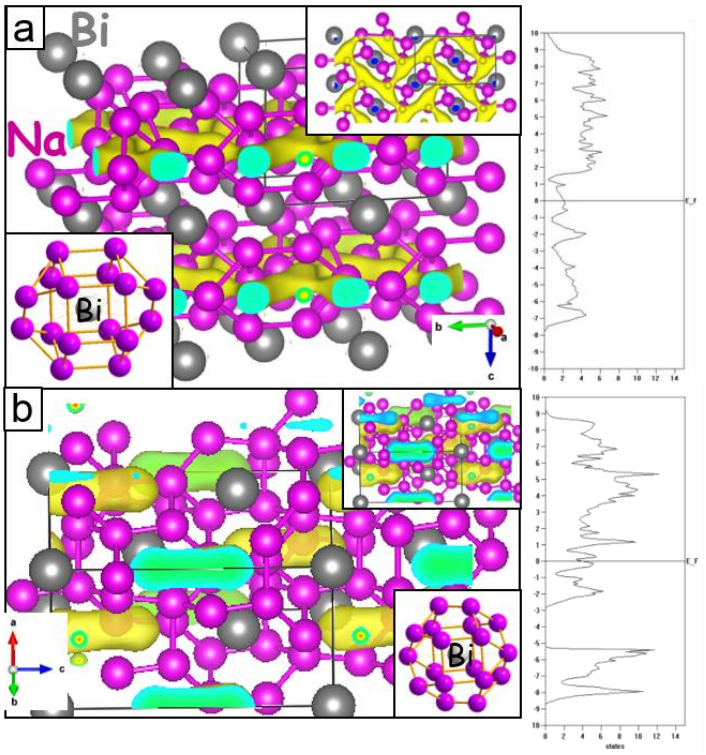

Figure S24. Electronic structure of Na_6Bi. Results taken from single point VASP calculations performed at the geometry reported in ref.14. (a) valence charge density (energy range -4 eV/0.0 eV with respect to the Fermi level) of Pbam-Na_6Bi plotted as 0.02 e/a.u. isosurface. The bottom-left inset shows the coordination sphere of Bi. Na-Bi atoms were considered bonded when their distance was below 2.7 Å. Above such cutoff the shortest Na-Bi distances were longer than 4 Å for both structures. The top-right panel shows the view along the c axis. (b) valence charge density (energy range -4 eV/0.0 eV with respect to the Fermi level) of R-3m-Na_6Bi plotted as 0.02 e/a.u. isosurface. The bottom-right inset shows the coordination sphere of Bi. The top-right panel shows 0.01 isosurface. Note that the valence charge density is still localized in the interstices even when the isovalue is halved. For both pictures, the corresponding DOS is displayed on the right and shows a good agreement with the ones reported in ref. 14.

ESI 6. STRUCTURES AND DENSITY OF STATES FOR Li_5B

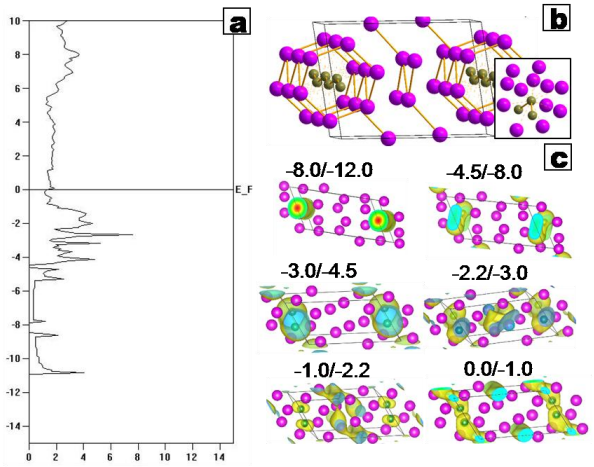

Figure S25. Density of states (a) and crystal structure (b) for $P2_1/m$-Li_5B at 100 GPa (B atoms represented as green spheres). In (a) the horizontal axis reports the density of states (eV^{-1}), while the vertical axis indicates the energy (eV, with respect to the Fermi level). The inset in (b) shows the coordination of the only symmetry-independent B atom (the Li-B atoms were considered bonded when their distance was lower than 2.5 Å). In (c) we show the charge density corresponding to a given energy range of the DOS (reported above each picture) as yellow isosurfaces. The isovalue used was 0.015 a.u. for all of them, except for the 0.0/-1.0 and -3.0/-2.2 ranges, for which the density was less than 0.015 a.u. everywhere and therefore we employed an isovalue of 0.005 a.u.

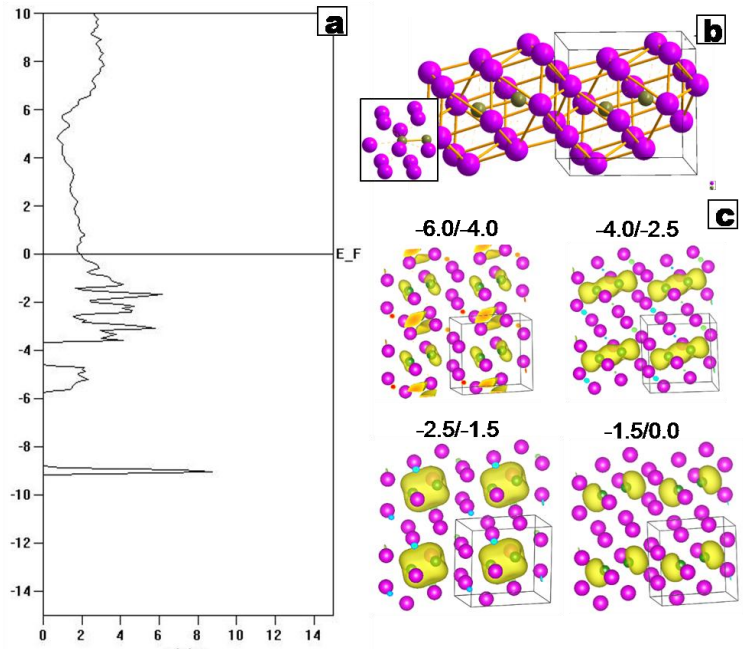

Figure S26. Density of states (a) and crystal structure (b) for P-1-Li_5B at 100 GPa. In (a) the horizontal axis reports the density of states (eV^{-1}), while the vertical axis indicates the energy (eV , with respect to the Fermi level). The inset in (b) shows the coordination of the only symmetry-independent B atom (the Li-B atoms were considered bonded when their distance was lower than 2.5 Å). In (c) we show the charge density

corresponding to a given energy range of the DOS (reported above each picture) as yellow isosurfaces (isovalue =0.015 a.u.).

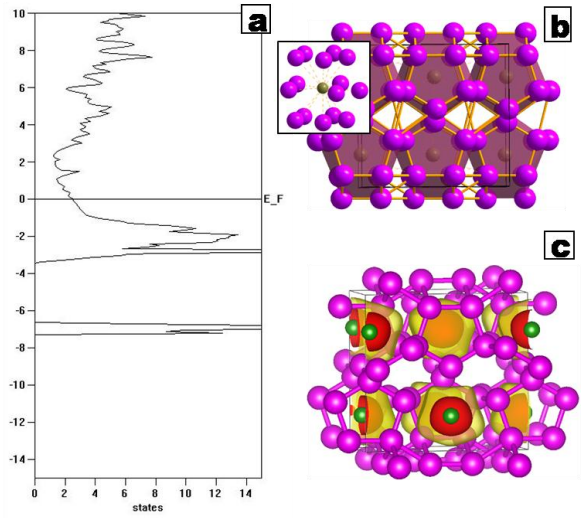

Figure S27. Density of states (a) and crystal structure (b) for Cmma-Li_5B at 100 GPa. In (a) the horizontal axis reports the density of states (eV^{-1}), while the vertical axis indicates the energy (eV, , with respect to the Fermi level). The inset in (b) shows the coordination of the only symmetry-independent B atom (the Li-B atoms were considered bonded when their distance was lower than 2.5 Å). In (c) we show the charge density corresponding to the valence band as yellow and red isosurfaces, whose isovalues are 0.03 a.u. and 0.05 a.u., respectively.

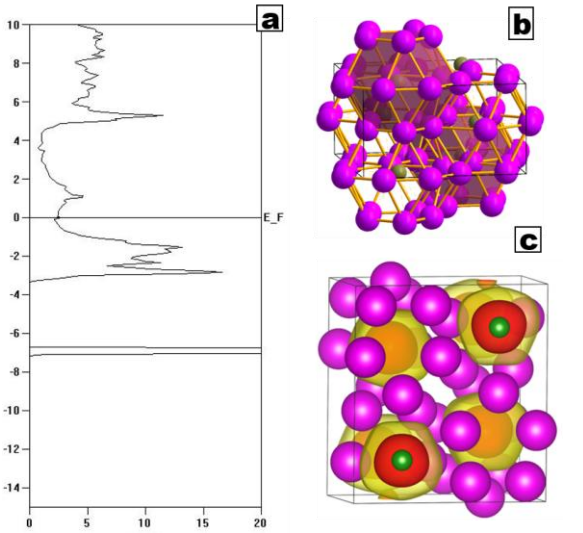

Figure S28. Density of states (a) and crystal structure (b) for Cmcm-Li_5B at 100 GPa. In (a) the horizontal axis reports the density of states (eV^{-1}), while the vertical axis indicates the energy (eV, with respect to the Fermi level). In (b) the polyhedra highlight the coordination sphere of the only symmetry-independent B atom (the Li-B atoms were considered bonded when their distance was lower than 2.5 Å). In (c) we show the

charge density corresponding to the valence band as yellow and red isosurfaces, whose isovalues are 0.03 a.u. and 0.05 a.u., respectively.

ESI 7. B3LYP AND M06L RESULTS FOR Imma-Na_2Cl

In this section, we present the results on Imma-Na_2Cl obtained using B3LYP and M06L DFT functionals. We also point out that open-shell calculations carried out using a starting guess with one unpaired electron on each Cl atom result in the same wavefunction as the one obtained from closed-shell calculations (the magnetic moment on each atom is lower than $5 \cdot 10^{-4}$, and the energy was unchanged within $1 \cdot 10^{-5}$ Hartree). This holds true for all three DFT functionals tested.

Table S10. Bader atomic volumes and charges for Imma-Na_2Cl at 300 GPa as obtained from B3LYP[15],[16] and M06L[17] calculations. For B3LYP, to obtain the SCF convergence, we had to use the 'single-polarization' basis functions (from ref. 3), as well as very high TOLINTEG values: 20,20,20,20,38 (see section ESI 1.2).

	Na		Cl	
Imma-Na_2Cl	charge	Volume [$bohr^3$]	charge	Volume [$bohr^3$]
B3LYP	0.70	28.81	-1.41	82.44
M06L	0.66	29.35	-1.31	81.37

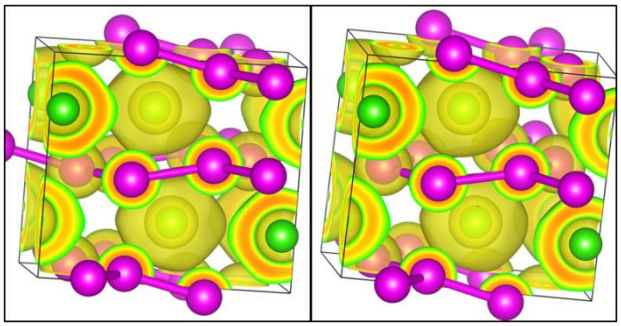

Figure S29. ELF distribution (0.5 isosurface) for Imma-Na_2Cl as obtained from B3LYP (left) and M06L (right) calculations. The total population (core+ monosynaptic valence ELF basins) of Cl atoms is 19.0 in both cases.

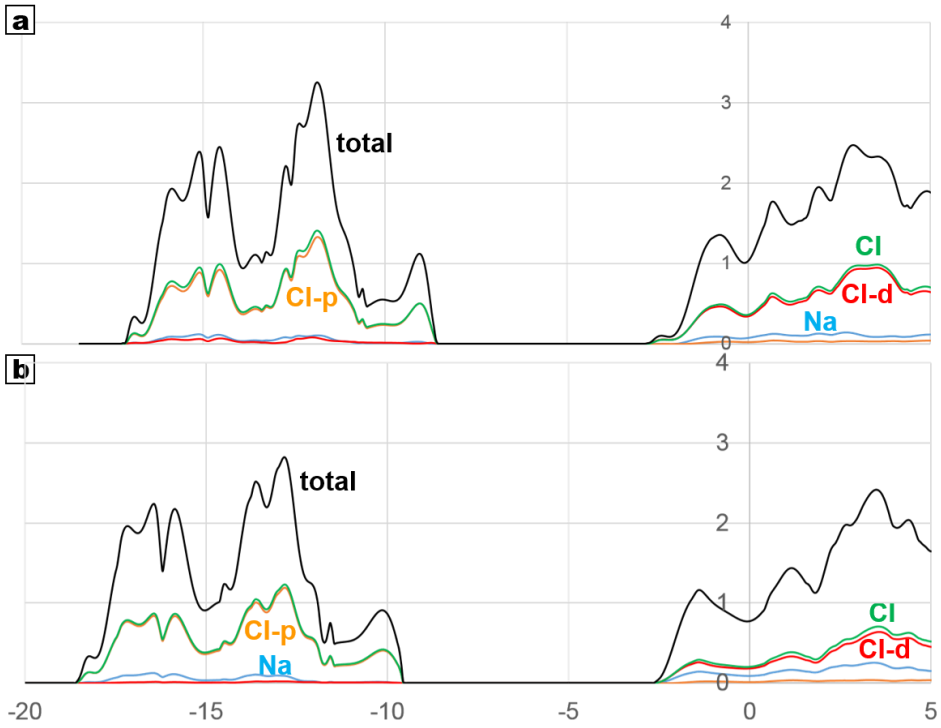

Figure S30. DOS of Imma-Na_2Cl obtained from M06L (a) and B3LYP (b) calculations. For the latter, the adopted contraction coefficients (see Sect. S1.2) were 1.69 and 3.24 for Cl and Na, respectively, while for M06L calculation we used the same contraction coefficients as for the PBE calculations (1.44 and 2.89). Horizontal and vertical axis report Energy (eV, with respect to Fermi level) and number of states (eV^{-1}), respectively.

REFERENCES

[1]W. Zhang, A. R. Oganov, A. F. Goncharov, Q. Zhu, S. E. Boulfelfel, A. O. Lyakhov, E. Stavrou, M. Somayazulu, V. B. Prakapenka and Z. Konopkova, *Science,* 2013, **342**, 1502-1505.

[2] CRYSTAL14: R. Dovesi, R. Orlando, A. Erba, C. M. Zicovich-Wilson, B. Civalleri, S. Casassa, L. Maschio, M. Ferrabone, M. De La Pierre, P. D'Arco, Y. Noel, M. Causa, M. Rerat and B. Kirtman, *Int. J. Quantum Chem,*. 2014, **114**, 1287-1317. Manual avilable at: http://www.crystal.unito.it/Manuals/crystal14.pdf

[3] M. F. Peintinger, D. V. Oliveira, and T. Bredow, *J. Comput. Chem.,* 2013, **34**, 451-459.

[4] D. E. Woon and T. H. Dunning. *J. Chem. Phys*., 1994, **100**, 2975.

[5] see http://www.theochem.unito.it/crystal_tuto/mssc2013_cd/tutorials/topond_2013/topond_manual.pdf and references therein

[6] O. Otero-de-la-Roza, E. R. Johnson and V. Luaña, *Computer Physics Communications,* 2014, **185**(3), 1007–1018.

[7] M. Yu, and D. R. Trinkle, *J. Chem. Phys.,* 2011, **134**, 064111.

[8] G. Saleh, L. Lo Presti, C. Gatti, D. Ceresoli *J. Appl. Cryst*., 2013, **46**, 1513-1517

[9] a) A. R. Oganov and C. W. Glass, *J. Chem. Phys.,* 2006, **124**, 244704. b) A. O. Lyakhov, A. R. Oganov, H. T. Stokes and Q. Zhu, *Comp. Phys. Comm.,* 2013, **184**, 1172-1182. c) A. R. Oganov, A. O. Lyakhov and M. Valle, *Accounts of Chemical Research,* 2011, **44**(3), 227–237.

[10]A. Togo, F. Oba, and Isao Tanaka, *Phys. Rev. B*, 2008, **78**, 134106.

[11] W. L. Cao, C. Gatti, P. J. MacDougall and R. F. W. Bader, *Chem. Phys. Lett.,* 1987, **141**, 380-385.

[12] C. Gatti, *Z. Kristallogr*., 2005**, 220**, 399–457

[13] A. Zunger, *Phys. Rev. B* 1980, **22**, 5839-5872.

[14] X. Cheng, R. Li, D. Li, Y. Li and X.-Q. Chen, *Phys. Chem. Chem. Phys.,* 2015, **17**, 6933- 6947.

[15] A. D. Becke, *J.Chem.Phys.* 1993, **98**, 5648-5652

[16] C. Lee, W. Yang and R. G. Parr, *Phys. Rev. B,* 1998, **37**, 785-789.

[17] Y. Zhao, D. G. Truhlar, *J. Chem. Phys.,* 2006, **125**,194101.